PAPER

Comparative study of ferromagnetic hybrid (manganese zinc ferrite, nickle zinc ferrite) nanofluids with velocity slip and convective conditions

View the article online for updates and enhancements.

Physica Scripta

PAPER

Comparative study of ferromagnetic hybrid (manganese zinc ferrite, nickle zinc ferrite) nanofluids with velocity slip and convective conditions

Tie-Hong Zhao[1], M Ijaz Khan[2] ◉, Sumaira Qayyum[3], R Naveen Kumar[4], Yu-Ming Chu[5,6,*] and B C Prasannakumara[4,*] ◉

1   Department of Mathematics, Hangzhou Normal University, Hangzhou 311121, People's Republic of China
2   Department of Mathematics and Statistics, Riphah International University I-14, Islamabad 44000, Pakistan
3   Department of Mathematics, Quaid-I-Azam University 45320, Islamabad 44000, Pakistan
4   Department of Mathematics, Davangere University, Davangere , Karnataka, India
5   Department of Mathematics, Huzhou University, Huzhou 313000, People's Republic of China
6   Hunan Provincial Key Laboratory of Mathematical Modeling and Analysis in Engineering, Changsha University of Science & Technology, Changsha 410114, People's Republic of China
*   Authors to whom any correspondence should be addressed.

E-mail: chuyuming@zjhu.edu.cn and prasannakumarabc@davangereuniversity.ac.in

Abstract

The current article explores the effect of viscous dissipation on the hybrid nanofluid flow over a stretching sheet. Further, different nanoparticles can be used to enhance the thermal conductivity of the fluid. The resultant suspension is examined with the effect of velocity slip. The velocity slip effect is incorporated in the boundary condition of the momentum equation. Heat transfer analysis is done in presence of convective conditions and thermal radiation. Comparative study of different hybrid nanofluids and nanofluid is considered. Here we have chosen manganese Zinc ferrite $MnZnFe_2O_4$ and Nickle Zinc ferrite $NiZnFe_2O_4$ as nanoparticles in base fluids Kerosene oil and engine oil. Mathematical modeling of the present flow system is illustrated and solved by the shooting built-in method. Graphs for velocity, temperature, skin friction and Nusselt number are presented for different parameters. Here we noticed that velocity profile of $MnZnFe_2O_4 - NiZnFe_2O_4 - C_{10}H_{22} - C_8H_{18}$ is maximum as compared to other hybrid nanofluids. Velocity and temperature have opposite effects against slip parameter. The temperature of the fluid rises with Biot number and thermal radiation.

Introduction

In heat transfer, equipment fluids are often used as heat carriers. A few instances of important equipments of heat passage of fluids include aeronautics and vehicular freezing frameworks in manufacturing fields, freezing and hydronic warming frameworks in structures, material, nourishments and synthetics. When two or more nanofluids are mixed with conventional base fluids like water or ethylene glycol or kerosene or engine oil possess high thermal conductivity and this mixture of dual nanoparticles in base fluids are called as hybrid nanofluids. Recently, several researchers examined the nanofluid and hybrid nanofluids flow through diverse surfaces. Rashad *et al* [1] explored the magnetic field and internal heat generation effects on the free convective stream of nanoliquid in a rectangular cavity filled with porous medium. Mohebbi and Rashidi [2] examined the natural convective stream of nanofluid in an L-shaped enclosure with a heating obstacle. Daniel *et al* [3–5] exemplified the viscous dissipation and radiation effects on magnetohydrodynamic (MHD) flow of nanofluid with chemical reaction through diverse surfaces. Zeeshan and Majeed [6] illustrated the analysis of heat transfer on a ferromagnetic fluid flow through a stretching sheet. Muhammad and Nadeem [7] scrutinized the convective heat transference elevated in boundary layer flow regions via ferrite nanoparticles. Yang *et al* [8] utilized the

Magnetite and Manganese zinc ferrite nanoparticles suspended in dual diverse carrier fluids to illustrate the influences on the heat transference and friction drag. Jayadevamurthy *et al* [9] numerically explored the bioconvective stream of hybrid nanofluid past a moving rotating disk. Kumar *et al* [10]. deliberated the magnetic dipole effect on ferromagnetic hybrid nanoliquid stream past an extending cylinder.

The fluid flow with viscous dissipation effect is of great importance among scientists. Effects of viscous dissipation are often neglected but its presence becomes significant when liquid viscosity is high. It changes the temperature distributions by playing a key role like an energy source which leads to affect heat transfer rates. Recently, Daniel *et al* [11] exemplified the viscous dissipation and radiation effects on magnetohydrodynamic (MHD) flow of nanofluid with chemical reaction. Farooq *et al* [12] scrutinized the peristaltic activity of different nanoparticles in viscous fluid on taking account of radiation and slip effects. Hayat *et al* [13] scrutinized the hydrodynamic Darcy-Forchheimer viscous liquid flow through an extending surface. Shehzad *et al* [14] examined the impact of Hall current on instable viscous liquid through the oscillatory spinning disk.

The no-slip boundary constraint is one of the focal standards of the 'Navier–Stokes hypothesis'. Yet, there are numerous conditions where this constraint does not work. The slip condition can apply to particle suspended liquids like nanofluids or foams and single-phase fluids as well. The non-adherence strong liquid interface movement which is additionally called as velocity slip which is a hydrodynamic term that has been inspected under certain conditions. Vinita and Poply [15] analytically depicted the consequences of velocity slip and heat production on the hydrodynamic slip flow of nanofluid with the help of a stretching cylinder. The impact of ohmic effect and viscous dissipation on the MHD flow of nanoliquid through a cylinder on taking account of thermal and velocity slip effects was scrutinized by Mishra and Kumar [16]. Ramesh *et al* [17] discussed the heat transference in hybrid nanofluid flow with chemical reactions and slip effects. Khan *et al* [18] examined the Darcy-Forchheimer second-order velocity slip flow of hybrid nanofluid between dual gyrating disks. Khan *et al* [19] used the above conditions on Carreau-Yasuda liquid and studied the rate of entropy generation.

In modern engineering, many processes take place at high temperatures and the knowledge of radiation transfer is crucial to the development of proper equipment. Atomic power plants, electric turbines, rockets, satellites, and space vehicles are such regional conditions. Studying the effects of radiation on different types of flow is extremely difficult. From past decades, several researchers examined the effect of radiation on diverse fluid streams over diverse surfaces [20–22]. The stagnation point flow of Casson liquid over a stretching sheet with radiation effect was scrutinized by Ramesh *et al* [23]. Prasannakumara *et al* [24] explored the mass and heat transference in Sisko nano liquid flow over a stretching sheet on taking account of radiation effect and chemical reaction. Kumar *et al* [25] deliberated the impact of radiation effect on hybrid nanofluid flow with CNT's as nanoparticles. Nadeem *et al* [26] investigated the chemically reactive Sisko nanofluid instigated by a rotating disk saturated with the non-Darcy permeable medium. Jamaludin *et al* [27] scrutinized the convective flow of ferrofluid through a nonlinearly moving surface.

Convective boundary conditions play a vital role in fluid flow through several surfaces. Many researchers used convective boundary constraints to study different fluid flows through several surfaces. Recently, Chamkha *et al* [28] studied the influence of the magnetic effect along with viscous dissipation in nanofluid flow on taking account of homogeneous and Heterogeneous chemical reactions. Jyothi *et al* [29] discussed the water-based SWCNT and MWCNT flow through stretchable gyrating disks. Here the influence of radiation effect and magnetic field are considered along with convective boundary constraint. Khan *et al* [30] exposed the influence of activation energy on nanofluid flow with gyrotactic microbes and convective boundary constraint. The influence of viscous dissipation on the MHD flow of a tangent hyperbolic nanofluid was explored by Atif *et al* [31]. The heat transport in a non-Newtonian nanofluid with radiation effect was scrutinized by Reddy *et al* [32].

In view of the above literature survey, it is obvious to the best of the writer's knowledge, that no efforts have far been initiated concerning viscous dissipation and radiation effects on stream of a hybrid nanoliquid over a stretching sheet. Hence in this investigation, we scrutinized a hybrid nanoliquid stream over a stretching sheet on taking account of velocity slip and convective boundary conditions. Further, we have done a comparative study on a different combination of nanoparticles suspension in diverse carrier liquids.

Mathematical formulation

Here we have considered two-dimensional steady flow of different hybrid nanofluids. Slip flow is considered at boundary condition of momentum equation. Convective boundary condition and thermal radiation is also considered in thermal equation. Sheet is stretched with stretching rate S. Here we have chosen manganese Zinc ferrite $MnZnFe_2O_4$ and Nickle Zinc ferrite $NiZnFe_2O_4$ as nanoparticles and Kerosene oil and engine oil are used as base fluids. figure 1 describes the flow geometry of the problem.

Equation (1) is the continuity equation which shows that in flow is equals to out flow. Equation (2) is momentum equation which holds the conservation law of momentum. First term on left hand side of
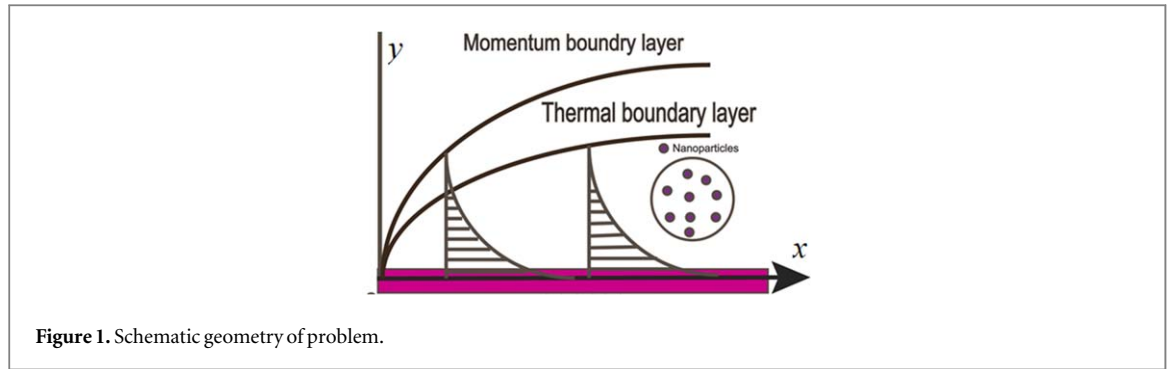
Figure 1. Schematic geometry of problem.

equation (2) is due to inertial forces, first term on right hand side is due to pressure force and second term is due to viscous forces. Here hybrid nanofluids are studied comparatively in detail. Equation (3) holds the conservation law of energy. Here last term of right-hand side shows the additional effect of thermal radiation. From all above assumptions flow equations are presented below ([3, 4] and [7]):

$$\frac{\partial u}{\partial x} + \frac{\partial v}{\partial y} = 0 \tag{1}$$

$$\rho_{hnf}\left(u\frac{\partial u}{\partial x} + v\frac{\partial u}{\partial y}\right) = -\frac{\partial p}{\partial x} + \mu_{hnf}\frac{\partial^2 u}{\partial y^2} \tag{2}$$

$$(\rho C_p)_{hnf}\left(u\frac{\partial T}{\partial x} + v\frac{\partial T}{\partial y}\right) = k_{hnf}\frac{\partial^2 T}{\partial y^2} + \frac{16\sigma^* T_\infty^3}{3k^*}\frac{\partial^2 T}{\partial y^2} \tag{3}$$

The corresponding boundary conditions are as follow:

$$u = Sx + U_{slip}, \, v = 0, \, k_{hnf}\frac{\partial T}{\partial y} = -h_1(T_f - T) \quad u \to 0, \, T \to T_\infty \tag{4}$$

$$where$$

$$U_{slip} = \lambda_1\frac{\partial u}{\partial y} \tag{5}$$

Here, (u, v) are velocity vector, (x, y) are Cartesian coordinates, T is temperature, T_∞ is ambient temperature, T_f is surface temperature, λ_1 is slip coefficient, h_1 is heat transfer coefficient. The fallowing similarity transformations are considered in the modelling ([4, 5]):

$$\xi = y\sqrt{\frac{S}{\nu_f}}, \, u = Sxf'(\xi), \, v = -\sqrt{S\nu_f}f(\xi), \, \theta(\xi) = \frac{T - T_\infty}{T_w - T_\infty} \tag{6}$$

where $\nu_f = \nu_{f1} + \nu_{f2}$ in case of two base fluid.

The continuity equation (equation (1)) is satisfied after employing equation (6), the remaining reduced equations in dimensionless form are as follow:

$$\frac{f'''}{(1 - \phi_1)^{5/2}(1 - \phi_2)^{5/2}A_1} + ff'' - f'^2 = 0 \tag{7}$$

$$\frac{1}{\text{Pr}A_2}\left[\frac{k_{hnf}}{k_{f1} + k_{f2}} + R\right]\theta'' + f\theta' = 0 \tag{8}$$

The corresponding reduced boundary conditions are:

$$f'(0) = 1 + L_1 f''(0), \, f(0) = 0, \, \theta'(0)\frac{k_{hnf}}{k_{f1} + k_{f2}} = -B_1(1 - \theta(0))$$

$$f'(\infty) \to 0, \, \theta(\infty) \to 0 \tag{9}$$

Where, R is radiation parameter, Pr is Prandtl number, L_1 is slip parameter and B_1 is Biot number.

$$R = \frac{16\sigma^* T_\infty^3}{3k^*(k_{f1} + k_{f2})}, \, \text{Pr} = \frac{((\rho C_p)_{f1} + (\rho C_p)_{f2})\nu_f}{k_{f1} + k_{f2}}, \, L_1 = \lambda_1\sqrt{\frac{S}{\nu_f}}, \, B_1 = \frac{h_1}{k_{f1} + k_{f2}}\sqrt{\frac{\nu_f}{S}},$$

$$A_1 = \frac{\rho_{hnf}}{(\rho_{f1} + \rho_{f2})}, \, A_2 = \frac{(\rho C_p)_{hnf}}{((\rho C_p)_{f1} + (\rho C_p)_{f2})}. \tag{10}$$

Table 1. Thermo physical properties of base fluid and ferrite nanoparticles ([7, 10] and [33]).

Physical properties	ρ (kg m^{-3})	C_p (J/kgK)	k (W mK^{-1})	Pr
C_8H_{18}	890	1868	0.145	12900
$C_{10}H_{22}$	783	2090	0.15	21
$MnZnFe_2O_4$	4700	1050	3.9	—
$NiZnFe_2O_4$	4800	710	6.3	—

The physical quantities of engineering interests skin friction and Nusselt number are given by:

$$C_{fx} = \frac{\tau_w}{(\rho_{f1} + \rho_{f2})U_w^2}, \; Nu_x = \frac{xq_w}{(k_{f1} + k_{f2})(T_w - T_\infty)} \tag{11}$$

Where

$$\tau_w = (\mu_{f1} + \mu_{f2})\frac{\partial u}{\partial y}, \; q_w = -k_{hnf}\frac{\partial T}{\partial y} - \frac{16\sigma^* T_\infty^3}{3k^*}\frac{\partial T}{\partial y} \tag{12}$$

The dimensionless forms of skin friction and Nusselt number are given by:

$$Re^{0.5}\, C_{fx} = f''(0), \; Nu_x\, Re^{-0.5} = -\left(\frac{k_{hnf}}{(k_{f1} + k_{f2})} + R\right)\theta'(0) \tag{13}$$

Results and discussion

This segment comprises the importance of physical explanation of various dimensionless parameters on the boundary value problem. The complete examination is performed by considering two distinctive nanoparticles of ferrites in particular, nickel zinc ferrite and manganese zinc ferrite with kerosene oil and Engine oil (C_8H_{18}) as base fluids. The thermophysical properties of ferrite nano particles and base fluids are given in tables 1–3. The reduced ODEs are solved numerically and analysed with the help of graphs. The rate of heat transportation phenomenon is portrayed in the resulting hybrid nanofluids. The impact of dimensionless parameters such as slip, radiation parameter, Prandtl number and Biot number are deliberated. The pictorial results of the velocity gradient, temperature profile and skin friction coefficient are found to get an obvious insight of the existing boundary layer flow problem.

Velocity distribution
The variation in velocity distribution for several influencing parameters are displayed in figures 2–5. Figure 2 is depicted to scrutinize the movements of fluid particles in the absence of added effects for various special cases namely, $MnZnFe_2O_4$ and $NiZnFe_2O_4$ as nanoparticles with $C_{10}H_{22} - C_8H_{18}$ hybrid base fluid, $MnZnFe_2O_4$ and $NiZnFe_2O_4$ as nanoparticles suspended in C_8H_{18} as base fluid, $MnZnFe_2O_4$ and $NiZnFe_2O_4$ as nanoparticles suspended in kerosene oil as base fluid and $NiZnFe_2O_4$ as nanoparticle along with $C_{10}H_{22}$ as a base fluid. One can notice from the figure that, $MnZnFe_2O_4$ and $NiZnFe_2O_4$ as nanoparticles with $C_{10}H_{22}$-C_8H_{18} has higher velocity and $MnZnFe_2O_4$-$NiZnFe_2O_4$ as nanoparticles with $C_{10}H_{22}$ has lower velocity when compared to other cases. Figure 3 is portrayed to illustrate the influence of slip parameter subjected to velocity gradients for two different conditions namely, $MnZnFe_2O_4$ and $NiZnFe_2O_4$ as nanoparticles suspended in base fluid $C_{10}H_{22} - C_8H_{18}$. Figure reveals that the velocity of the fluid motion and related boundary layer thickness declines for increase in the value of slip parameter. From physical fact of sight, increase in slip parameter deteriorates in the saturation of the fixed surface due to the boundary layer in both the transverse and axial directions, which results in decay of velocity gradient. It is also observed that, the rate of decrease in velocity gradient is faster in $MnZnFe_2O_4$ and $NiZnFe_2O_4$ as nanoparticles suspended in C_8H_{18}. Figure 4 displays the distribution of velocity in the velocity boundary layer for diverse values of the slip parameter for two different cases with $MnZnFe_2O_4$ and $NiZnFe_2O_4$ as nanoparticles suspended in $C_{10}H_{22}$ as a base fluid and $NiZnFe_2O_4$ as nanoparticles with $C_{10}H22$ as a base fluid. Here, it is noticed that velocity gradient declines for enhance in values of slip parameter. Solution containing $MnZnFe_2O_4$ and $NiZnFe_2O_4$ as nanoparticles declines faster than the solution suspended with $NiZnFe_2O_4$ as nanoparticle. Physically, this infers that the frictional obstruction between the surface and liquid molecule increments. Therefore, the fluid velocity declines. Figure 5 delineates the impact of the nanoparticle solid volume fraction over two different solution containing $MnZnFe_2O_4$ and $NiZnFe_2O_4$ as nanoparticles with hybrid base fluid and C_8H_{18} base fluid respectively. It is noticed that the increased values of ϕ improves the axial velocity gradient. The impact of boundary layer thickness is to oppose

5

Table 2. Thermo physical properties of both $MnZnFe_2O_4 - NiZnFe_2O_4 - C_{10}H_{22}$ and $MnZnFe_2O_4 - NiZnFe_2O_4 - C_{10}H_{22} - C_8H_{18}$ ([7, 10] and [33]).

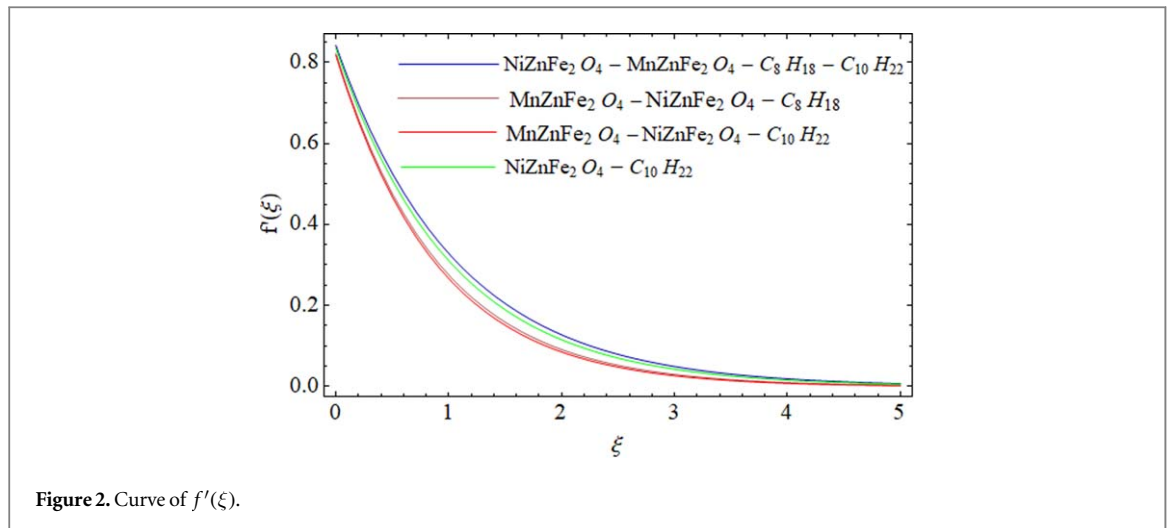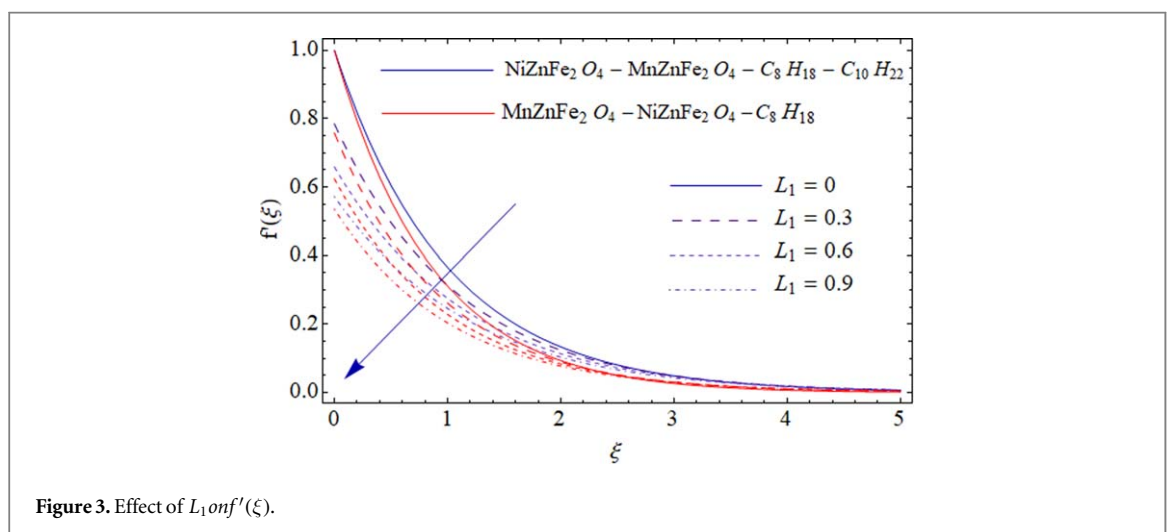| Properties	$MnZnFe_2O_4 - NiZnFe_2O_4 - C_{10}H_{22}$	$MnZnFe_2O_4 - NiZnFe_2O_4 - C_{10}H_{22} - C_8H_{18}$
Density ρ	$\frac{\rho_{hnf}}{\rho_f} = (1 - \phi_2)\left[(1 - \phi_1) + \phi_1 \frac{\rho_{s1}}{\rho_f}\right] + \phi_2 \frac{\rho_{s2}}{\rho_f}$	$\frac{\rho_{hnf}}{\rho_{f1} + \rho_{f2}} = (1 - \phi_2)\left[(1 - \phi_1) + \phi_1 \frac{\rho_{s1} + \rho_{s2}}{\rho_{f1} + \rho_{f2}}\right] + \phi_2 \frac{\rho_{s1} + \rho_{s2}}{\rho_{f1} + \rho_{f2}}$
Heat capacity ρC_p	$\frac{(\rho C_p)_{hnf}}{(\rho C_p)_f} = (1 - \phi_2)\left[(1 - \phi_1) + \phi_1 \frac{(\rho C_p)_{s1}}{(\rho C_p)_f}\right] + \phi_2 \frac{(\rho C_p)_{s2}}{(\rho C_p)_f}$	$\frac{(\rho C_p)_{hnf}}{(\rho C_p)_{f1} + (\rho C_p)_{f2}} = (1 - \phi_2)\left[(1 - \phi_1) + \phi_1 \frac{(\rho C_p)_{s1} + (\rho C_p)_{s2}}{\rho_{f1} + \rho_{f2}}\right] + \phi_2 \frac{(\rho C_p)_{s1} + (\rho C_p)_{s2}}{(\rho C_p)_{f1} + (\rho C_p)_{f2}}$
Viscosity μ	$\mu_{hnf} = \frac{\mu_f}{(1 - \phi_1)^{2.5}(1 - \phi_2)^{2.5}}$	$\mu_{hnf} = \frac{\mu_{f1} + \mu_{f2}}{(1 - \phi_1)^{2.5}(1 - \phi_2)^{2.5}}$
Thermal conductivity	$\frac{k_{hnf}}{k_{bf}} = \frac{(k_{s2} + 2k_{bf}) - 2\phi_2(k_{bf} - k_{s2})}{(k_{s2} + 2k_{bf}) + \phi_2(k_{bf} - k_{s2})},$	$\frac{k_{hnf}}{k_{bf1} + k_{bf2}} = \frac{((k_{s1} + k_{s2}) + 2(k_{bf1} + k_{bf2})) - 2\phi_2((k_{bf1} + k_{bf2}) - (k_{s1} + k_{s2}))}{((k_{s1} + k_{s2}) + 2(k_{bf1} + k_{bf2})) + \phi_2((k_{bf1} + k_{bf2}) - (k_{s1} + k_{s2}))},$
	$\frac{k_{bf}}{k_f} = \frac{(k_{s1} + 2k_f) - 2\phi_1(k_f - k_{s1})}{(k_{s1} + 2k_f) + \phi_1(k_f - k_{s1})}.$	$\frac{k_{bf}}{k_f} = \frac{((k_{s1} + k_{s2}) + 2(k_{f1} + k_{f2})) - 2\phi_1((k_{f1} + k_{f2}) - (k_{s1} + k_{s2}))}{((k_{s1} + k_{s2}) + 2(k_{f1} + k_{f2})) + \phi_1((k_{f1} + k_{f2}) - (k_{s1} + k_{s2}))}.$
Prandtl number	21	12921

Figure 2. Curve of $f'(\xi)$.

Figure 3. Effect of L_1 on $f'(\xi)$.

Table 3. Thermo physical properties of NiZnFe$_2$O$_4$ -C$_{10}$H$_{22}$ and MnZnFe$_2$O$_4$-NiZnFe$_2$O$_4$ -C$_{10}$H$_{22}$([7, 10] and [33]).

Properties	$NiZnFe_2O_4 - C_{10}H_{22}$	$MnZnFe_2O_4 - NiZnFe_2O_4 - C_8H_{18}$
Density ρ	$\frac{\rho_{nf}}{\rho_f} = (1-\phi)\left[(1-\phi) + \phi\frac{\rho_s}{\rho_f}\right]$	$\frac{(\rho C_p)_{hnf}}{(\rho C_p)_f} = (1-\phi_2)\left[(1-\phi_1) + \phi_1\frac{(\rho C_p)_{s1}}{(\rho C_p)_f}\right] + \phi_2\frac{(\rho C_p)_{s2}}{(\rho C_p)_f}$
Heat capacity ρC_p	$\frac{(\rho C_p)_{nf}}{(\rho C_p)_f} = (1-\phi)\left[(1-\phi) + \phi\frac{(\rho C_p)_s}{(\rho C_p)_f}\right]$	$\frac{(\rho C_p)_{hnf}}{(\rho C_p)_f} = (1-\phi_2)\left[(1-\phi_1) + \phi_1\frac{(\rho C_p)_{s1}}{(\rho C_p)_f}\right] + \phi_2\frac{(\rho C_p)_{s2}}{(\rho C_p)_f}$
Viscosity μ	$\mu_{nf} = \frac{\mu_f}{(1-\phi)^{2.5}}$	$\mu_{hnf} = \frac{\mu_f}{(1-\phi_1)^{2.5}(1-\phi_2)^{2.5}}$
Thermal conductivity	$\frac{k_{nf}}{k_f} = \frac{(k_s + 2k_f) - 2\phi(k_f - k_s)}{(k_s + 2k_f) + \phi(k_f - k_s)}$	$\frac{k_{hnf}}{k_{bf}} = \frac{(k_{s2} + 2k_{bf}) - 2\phi_2(k_{bf} - k_{s2})}{(k_{s2} + 2k_{bf}) + \phi_2(k_{bf} - k_{s2})}$,
		$\frac{k_{bf}}{k_f} = \frac{(k_{s1} + 2k_f) - 2\phi_1(k_f - k_{s1})}{(k_{s1} + 2k_f) + \phi_1(k_f - k_{s1})}$.
Prandtl number	21	12900

relative movement of the liquid. The effect of viscosity is to resist relative motion of the fluid. In fact, it plays a key role in momentum transfer between the layers of fluid, and it acts when there are movements between those layers. In liquids, it is due to the van der Waals forces between the molecules. Subsequently, the including nanoparticles and nanotubes into engine oil would build its thickness because of the connections between the particles and oil atoms. By expanding the number of strong particles in a particular measure of a liquid, bigger nanoclusters emerge because of van der Waals forces between the particles. These nano-clusters avert the crusade of oil layers on each other, pioneering to advanced augmentation in viscidness. Also, one can observe that solution subtended by MnZnFe$_2$O$_4$ and NiZnFe$_2$O$_4$ as nanoparticles with hybrid base fluid inclines faster.
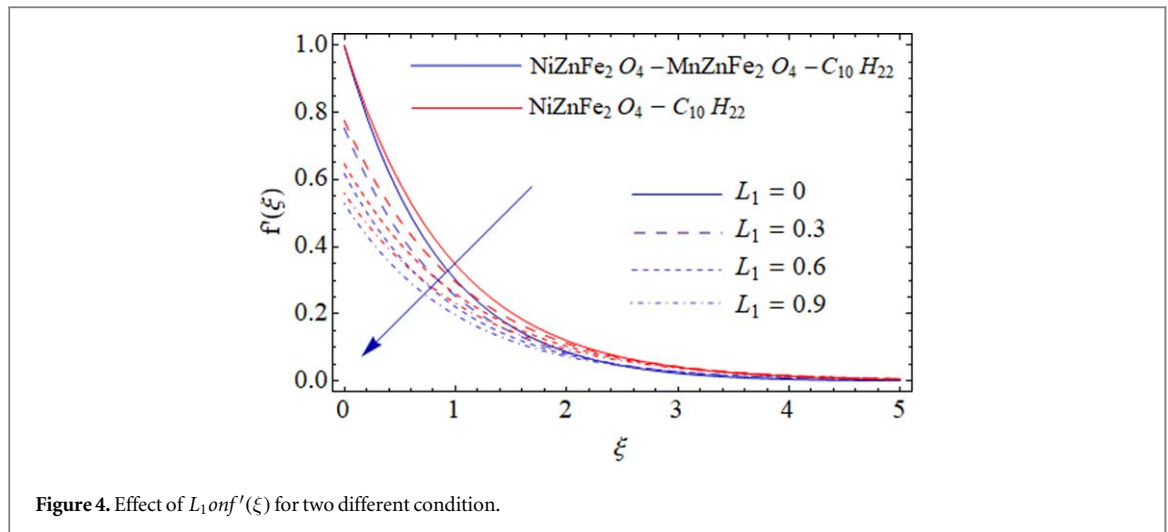
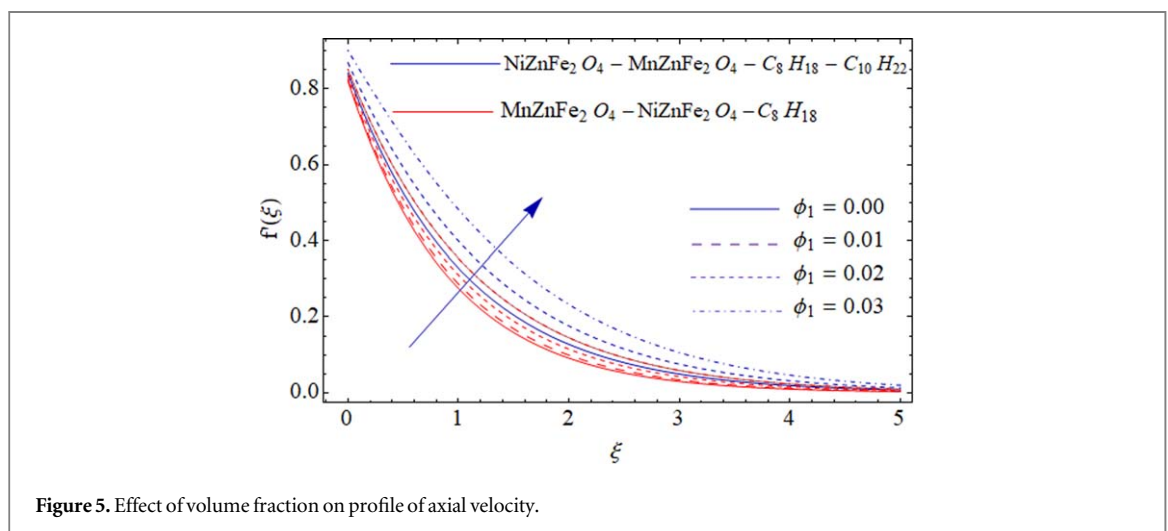**Figure 4.** Effect of L_1 on $f'(\xi)$ for two different condition.
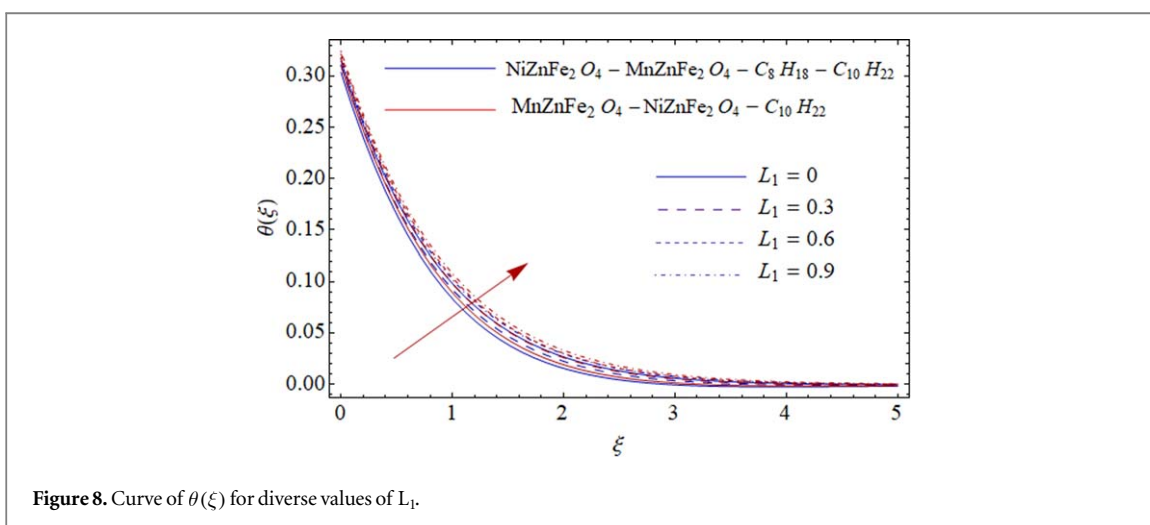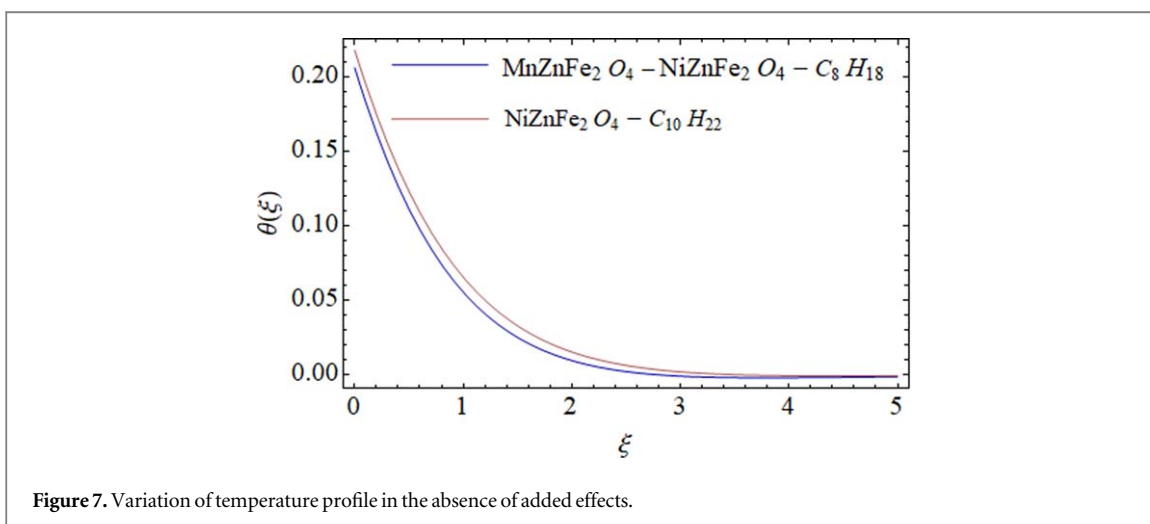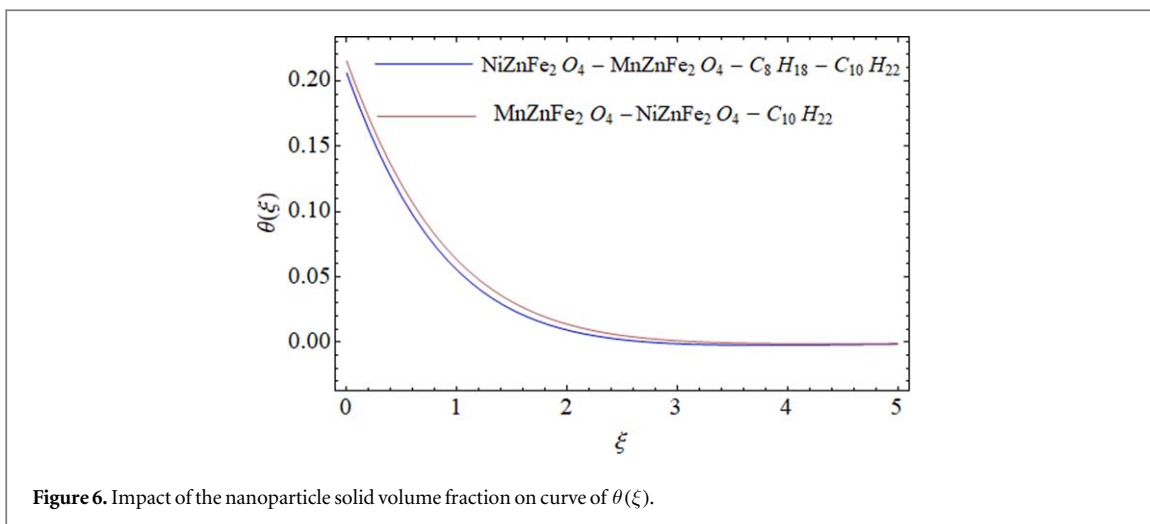

Figure 5. Effect of volume fraction on profile of axial velocity.

Table 4. Comparison table of $f''(0)$ and $f(\infty)$ for different values of slip parameter when .
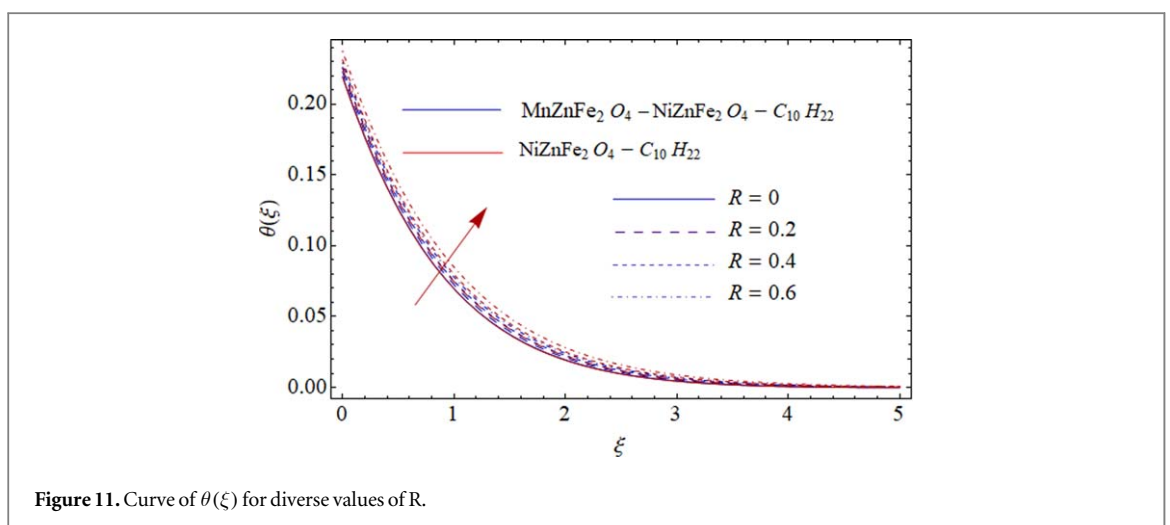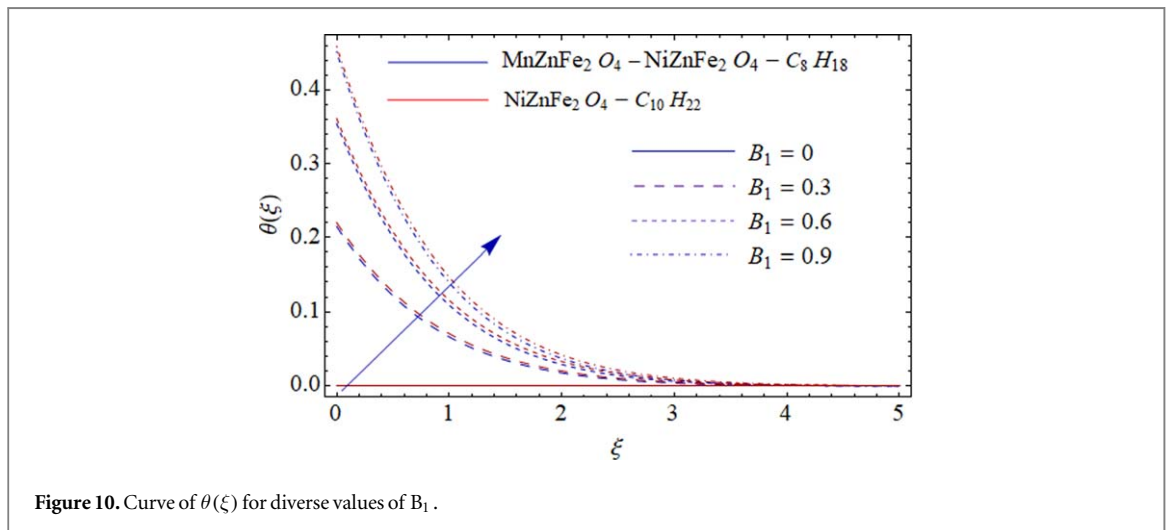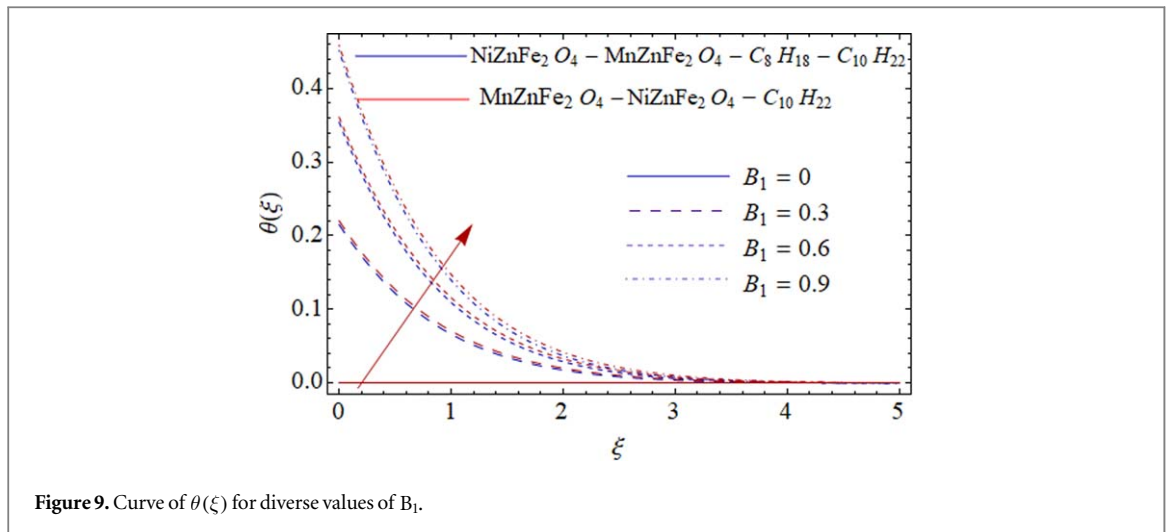
λ		0.0	0.3	1	2	5	30
Wang [34]	$f''(0)$	−1	−0.701	−0.430	−0.284	−0.145	−0.0438
	$f(\infty)$	1	0.887	0.748	0.652	0.514	0.322
Present	$f''(0)$	−1	−0.70125	−0.43014	−0.28412	−0.14585	−0.04384
	$f(\infty)$	1	0.88756	0.74895	0.65245	0.51458	0.32254

Thermal distribution

The variation in thermal distribution for several influencing parameters are displayed in figures 6–11. Plots of the thermal function in the absence of added effects for two different solutions subtended by ferrites nanoparticles with hybrid base fluid and $C_{10}H_{22}$ respectively, are shown in the figure 6. It is observed that, solution with $C_{10}H_{22}$ as a base fluid has higher thermal gradient when compared with hybrid base fluid subtended by ferrites nanoparticles. Figure 7 explains the change in thermal gradient due to the absence of added effects. $MnZnFe_2O_4$ and $NiZnFe_2O_4$ as nanoparticles suspended in engine oil as a carrier fluid has lower thermal gradient when compared with $NiZnFe_2O_4$ as nanoparticles with Engine oil as a base fluid. Figure 8 illustrates the change in thermal gradient in the interior of the boundary layer for several values of slip parameter for hybrid base fluid and base fluid kerosene oil both containing ferrites nanoparticles $MnZnFe_2O_4$ and $NiZnFe_2O_4$. It is noticed that the presence of the surface slipperiness affects temperature gradient, the enhance in values of slip parameter increases the thermal gradient and its related boundary layer thickness. Also, it is observed that base fluid kerosene oil suspended by ferrites nanoparticles $MnZnFe_2O_4$ and $NiZnFe_2O_4$ shows higher rate of increase when compared with hybrid base fluid suspended by ferrites nanoparticles $MnZnFe_2O_4$ and $NiZnFe_2O_4$. The

Figure 6. Impact of the nanoparticle solid volume fraction on curve of $\theta(\xi)$.

Figure 7. Variation of temperature profile in the absence of added effects.

Figure 8. Curve of $\theta(\xi)$ for diverse values of L_1.

heat transference at the surface diminishes with the expansion in estimation of slip boundary. This might be because of the way that the slip boundary diminishes the thermal conductivity of the nanofluid. Therefore, heat passage rate at the surface abatements, which raises the thickness of the thermal boundary layer. Figure 9 demonstrate the influence of Biot number subjected to thermal profile for two different solution containing ferrites nanoparticles along with kerosene oil as a base fluid. Physically, inclination in Biot number produces

Figure 9. Curve of $\theta(\xi)$ for diverse values of B_1.

Figure 10. Curve of $\theta(\xi)$ for diverse values of B_1 .

Figure 11. Curve of $\theta(\xi)$ for diverse values of R.

large heat transfer through convection which results in inclination of thermal field. Figure 10 illustrates the behaviour of thermal gradient over the influence of Biot number for suspended ferrites nanoparticles with C_8H_{18} as base fluid and $NiZnFe_2O_4$ nanoparticles with $C_{10}H_{22}$ as a base fluid respectively. Increase in Biot number increases the thermal profile. Also, rate of increase in hybrid based nanofluid is slower when compared
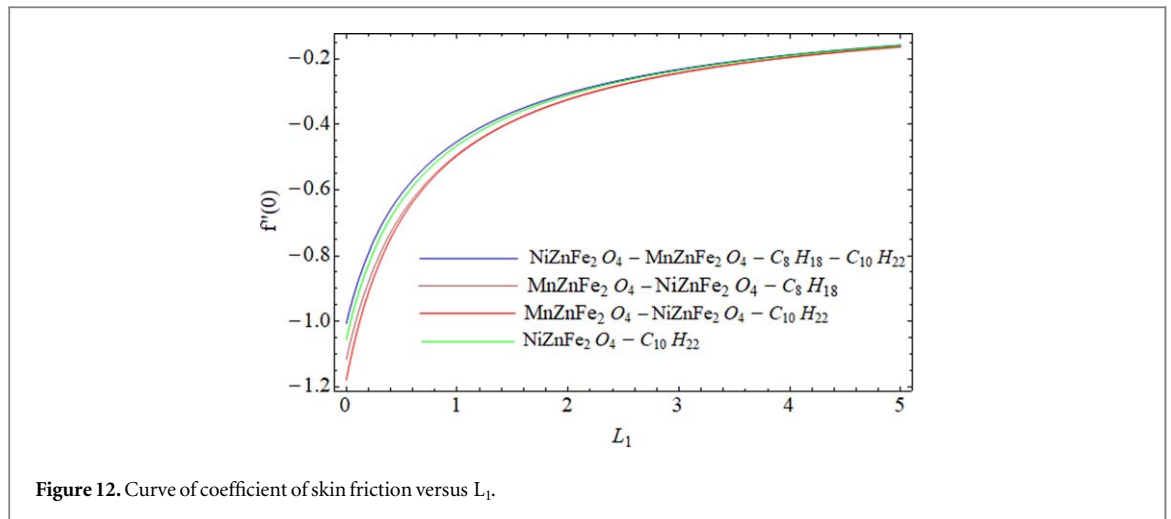
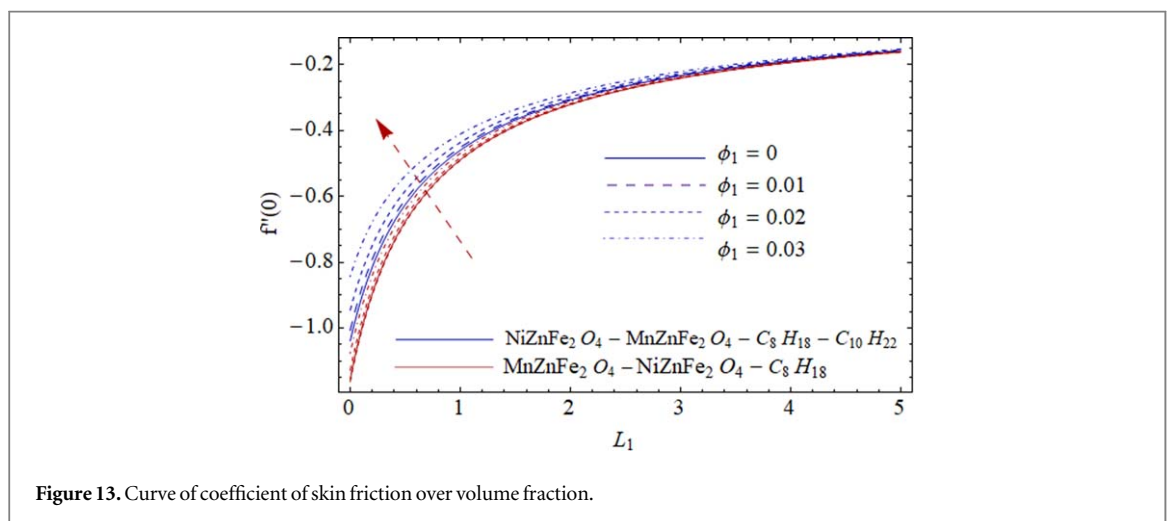**Figure 12.** Curve of coefficient of skin friction versus L_1.

Figure 13. Curve of coefficient of skin friction over volume fraction.

with kerosene oil as a base fluid suspended by ferrites nanoparticles (figure 9). Similar pattern in rate of increase can be observed for both hybrid nanofluid and nanofluid flow (figure 10). Physically, the more grounded convection brings about higher surface temperatures, making the thermal impact infiltrate further into the liquid. Figure 11 is prepared to disclose the impact of R on thermal gradient. To understand the importance of radiation parameter, a close observation is done over the thermal profile for both hybrid nonfluid and nanofluid subtended by ferrites nanoparticles with $C_{10}H_{22}$ as a base fluid. Also, it is noticed that increase in radiation parameter inclines the thermal gradient and thickness of its associated boundary layer gradually. The rate of increase in thermal profile for nanofluid containing ferrites nanoparticle $NiZnFe_2O_4$ is faster than hybrid nanofluid with ferrites nanoparticles $MnZnFe_2O_4$ and $NiZnFe_2O_4$. Since, heat radiation has a profound effect on the liquid temperature. Here, it is noted that the distribution of temperatures increases when the R is increased which in turn generates internal heat in the system. This is because the insertion of the coefficient decay by a rise in R which is responsible to the enhancement of thermal field.

Coefficient of skin friction and rate of heat transfer

Figures 12–15 displays the change in coefficient of skin friction and Nusselt number. The coefficient of skin friction and Nusselt number expressions are given in mathematical formulation section. Figure 12 is plotted to discuss the variation in coefficient of skin friction for several combination of nanoparticles with different combination of base fluids. One can observe from figure that skin friction coefficient of $MnZnFe_2O_4$-$NiZnFe_2O_4$-$C_{10}H_{22}$-C_8H_{18} is higher when compared to remaining nanoparticle mixture with single base fluid as shown in figure 12. It is because of the fact that the presence of ferrite nanoparticles in single base liquid diminishes the wall shear stress as related to the case when $C_{10}H_{22}$-C_8H_{18} based ferrite nanoparticles. Figure 13 is plotted to analyse the coefficient of skin friction for diverse values of volume fractions. One can observe from the figure that the uppermost wall shear stress is detected for $MnZnFe_2O_4$-$NiZnFe_2O_4$-$C_{10}H_{22}$-C_8H_{18} when compared to $MnZnFe_2O_4$-$NiZnFe_2O_4$-$C_{10}H_{22}$. This is because of the way that, the ferrite nanoparticles which bring about the enhancement of the thickness of the nanofluid inside the boundary layer and yet the wall shear stress increases. Figure 14 illustrates the variation in heat
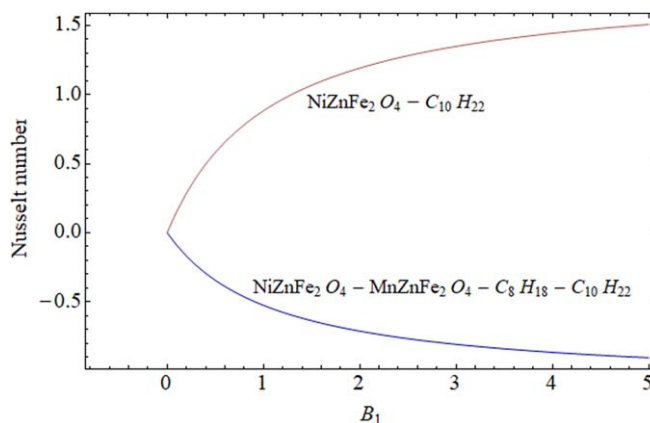
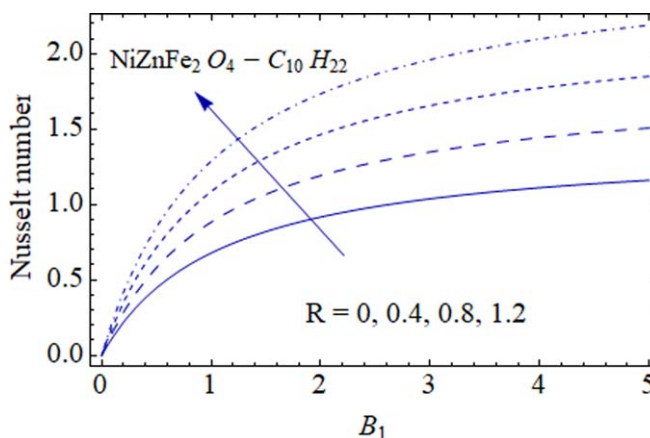**Figure 14.** Curve of Nusselt number versus B_1.

Figure 15. Curve of Nusselt number versus R.

transfer rate versus B_1. It is detected from figure that the rate of heat transference is lesser in $MnZnFe_2O_4$-$NiZnFe_2O_4$-$C_{10}H_{22}$-C_8H_{18} when compared to $NiZnFe_2O_4$-$C_{10}H_{22}$. The variation in rate of heat transfer $NiZnFe_2O_4$-$C_{10}H_{22}$in for diverse values of R is depicted in figure 15. One can observe from plot that enhancement in radiation effect increases the rate of heat transfer. Table 4 is constructed to show the validation of the problem by comparing our results in limiting case for $f''(0)$ and $f(\infty)$ with Wang [34] and we found the excellent agreement of results.

Conclusion

- Present paper is about hybrid nanofluids flow over a stretching sheet with velocity slip, thermal radiation and convective conditions. Key points of the present analysis are mentioned below:

- Velocity of $MnZnFe_2O_4$-$NiZnFe_2O_4$-$C_{10}H_{22}$-C_8H_{18} is dominant over all other nanofluids.

- Temperature of the fluid is more for $MnZnFe_2O_4$-$NiZnFe_2O_4$-$C_{10}H_{22}$ as compared to $MnZnFe_2O_4$-$NiZnFe_2O_4$-$C_{10}H_{22}$-C_8H_{18}.

- Temperature rises for higher slip parameter while decay in velocity is seen for greater slip parameter.

- Temperature is increasing function of Biot number and radiation parameter.

- Nusselt number is more for $NiZnFe_2O_4 - C_{10}H_{22}$ as compared to $MnZnFe_2O_4$-$NiZnFe_2O_4$-$C_{10}H_{22}$-C_8H_{18}.

- Magnitude of skin friction reduces for higher nanoparticles volume fraction.

Data availability statement

The data that support the findings of this study are available upon reasonable request from the authors.

ORCID iDs

M Ijaz Khan ⬤ https://orcid.org/0000-0002-9041-3292
B C Prasannakumara ⬤ https://orcid.org/0000-0003-1950-4666

References

[1] Rashad A M, Rashidi M M, Lorenzini G, Ahmed S E and Aly A M 2017 Magnetic field and internal heat generation effects on the free convection in a rectangular cavity filled with a porous medium saturated with Cu–water nanofluid *Int. J. Heat Mass Transf.* **104** 878–89

[2] Mohebbi R and Rashidi M M 2017 Numerical simulation of natural convection heat transfer of a nanofluid in an L-shaped enclosure with a heating obstacle *J. Taiwan Inst. Chem. Eng.* **72** 70–84

[3] Daniel Y S, Aziz Z A, Ismail Z and Salah F 2018 Impact of thermal radiation on electrical MHD flow of nanofluid over nonlinear stretching sheet with variable thickness *Alex. Eng. J* **57** 2187–97

[4] Shagaiya Daniel Y, Abdul Aziz Z, Ismail Z and Salah F 2017 Effects of thermal radiation, viscous and Joule heating on electrical MHD nanofluid with double stratification *Chin. J. Phys.* **55** 630–51

[5] Daniel Y S, Aziz Z A, Ismail Z and Salah F 2017 Numerical study of entropy analysis for electrical unsteady natural magnetohydrodynamic flow of nanofluid and heat transfer *Chin. J. Phys.* **55** 1821–48

[6] Zeeshan A and Majeed A 2016 Heat transfer analysis of Jeffery fluid flow over a stretching sheet with suction/injection and magnetic dipole effect *Alex. Eng. J* **55** 2171–81

[7] Muhammad N and Nadeem S 2017 Ferrite nanoparticles Ni-ZnFe$_2$O$_4$, Mn-ZnFe$_2$O$_4$ and Fe$_2$O$_4$ in the flow of ferromagnetic nanofluid *Eur. Phys. J. Plus* **132** 377

[8] Yang J, Abdelmalek Z, Muhammad N and Mustafa M T 2020 Hydrodynamics and ferrite nanoparticles in hybrid nanofluid *Int. Commun. Heat Mass Transf.* **118** 104883

[9] Jayadevamurthy P G R, Rangaswamy N K, Prasannakumara B C and Nisar K S 2020 Emphasis on unsteady dynamics of bioconvective hybrid nanofluid flow over an upward–downward moving rotating disk Numerical Methods for Partial Differential Equationsn/a, no. n/a

[10] Kumar R N, Gowda R J P, Abusorrah A M, Mahrous Y M, Abu-Hamdeh N H, Issakhov A, Rahimi-Gorji M and Prasannakumara1,* B C 2021 Impact of magnetic dipole on ferromagnetic hybrid nanofluid flow over a stretching cylinder *Phys. Scr.* **96** 045215

[11] Daniel Y S, Aziz Z A, Ismail Z and Salah F 2017 Entropy analysis in electrical magnetohydrodynamic (MHD) flow of nanofluid with effects of thermal radiation, viscous dissipation, and chemical reaction *Theor. Appl. Mech. Lett.* **7** 235–42

[12] Farooq S, Ijaz Khan M, Waqas M, Hayat T and Alsaedi A Transport of hybrid type nanomaterials in peristaltic activity of viscous fluid considering nonlinear radiation, entropy optimization and slip effects *Comput. Methods Programs Biomed.* **184** 105086

[13] Hayat T, Khan S A, Alsaedi A and Fardoun H M 2020 Heat transportation in electro-magnetohydrodynamic flow of Darcy-Forchheimer viscous fluid with irreversibility analysis *Phys. Scr.* **95** 105214

[14] Shehzad S A, Abbas Z, Rauf A and Mushtaq T 2020 Effectiveness of Hall current and thermophysical properties in compressible flow of viscous fluid thorough spinning oscillatory disk *Int. Commun. Heat Mass Transf.* **116** 104678

[15] Vinita V and Poply V 2020 Impact of outer velocity MHD slip flow and heat transfer of nanofluid past a stretching cylinder *Mater. Today Proc.* **26** 3429–35

[16] Mishra A and Kumar M 2020 Velocity and thermal slip effects on MHD nanofluid flow past a stretching cylinder with viscous dissipation and Joule heating *SN Appl. Sci.* **2** 1–13

[17] Ramesh G K, Manjunatha S, Roopa G S and Chamkha A J 2020 Hybrid (ND-Co$_3$O$_4$/EG) nanoliquid through a permeable cylinder under homogeneous-heterogeneous reactions and slip effects *J. Therm. Anal. Calorim.* 1–11

[18] Khan M I, Kadry S, Chu Y-M and Waqas M 2020 Modeling and numerical analysis of nanoliquid (titanium oxide, graphene oxide) flow viscous fluid with second order velocity slip and entropy generation *Chin. J. Chem. Eng.* (https://doi.org/10.1016/j.cjche.2020.08.005)

[19] Ijaz Khan M, Alzahrani F, Hobiny A and Ali Z 2020 Estimation of entropy optimization in Darcy-Forchheimer flow of Carreau-Yasuda fluid (non-Newtonian) with first order velocity slip *Alex. Eng. J* **59** 3953–62

[20] Daniel Y S and Daniel S K 2015 Effects of buoyancy and thermal radiation on MHD flow over a stretching porous sheet using homotopy analysis method *Alex. Eng. J* **54** 705–12

[21] Daniel Y S, Zainal A A, Ismail Z, Salah F *et al* 2019 Thermal radiation on unsteady electrical MHD flow of nanofluid over stretching sheet with chemical reaction *Journal of King Saud University - Science* **31** 804–12

[22] Bhatti M M, Mishra S R, Abbas T and Rashidi M M 2018 A mathematical model of MHD nanofluid flow having gyrotactic microorganisms with thermal radiation and chemical reaction effects *Neural Comput. Appl.* **30** 1237–49

[23] Ramesh G K, Prasannakumara B C, Gireesha B J and Rashidi M M 2016 Casson fluid flow near the stagnation point over a stretching sheet with variable thickness and radiation. *J. Appl. Fluid Mech.* **9**

[24] Prasannakumara B C, Gireesha B J, Krishnamurthy M R and Kumar K G 2017 MHD flow and nonlinear radiative heat transfer of Sisko nanofluid over a nonlinear stretching sheet *Inform. Med. Unlocked* **9** 123–32

[25] Kumar R, Kumar R, Sheikholeslami M and Chamkha A J 2019 Irreversibility analysis of the three-dimensional flow of carbon nanotubes due to nonlinear thermal radiation and quartic chemical reactions *J. Mol. Liq.* **274** 379–92

[26] Nadeem S, Ijaz M and Ayub M 2020 Darcy–Forchheimer flow under rotating disk and entropy generation with thermal radiation and heat source/sink *J. Therm. Anal. Calorim.*

[27] Jamaludin A, Naganthran K, Nazar R and Pop I 2020 Thermal radiation and MHD effects in the mixed convection flow of Fe$_3$O$_4$–water ferrofluid towards a nonlinearly moving surface *Processes* **8** 95

[28] Chamkha A J, Rashad A M, RamReddy C and Murthy P 2014 Viscous dissipation and magnetic field effects in a non-Darcy porous medium saturated with a nanofluid under convective boundary condition *Spec. Top. Rev. Porous Media Int. J.* **5** 27–39

[29] Jyothi K, Reddy P S and Reddy M S 2018 Influence of magnetic field and thermal radiation on convective flow of SWCNTs-water and MWCNTs-water nanofluid between rotating stretchable disks with convective boundary conditions *Powder Technol.* **331** 326–37

[30] Khan M I, Haq F, Khan S A, Hayat T and Khan M I 2020 Development of thixotropic nanomaterial in fluid flow with gyrotactic microorganisms, activation energy, mixed convection *Comput. Methods Programs Biomed.* **187** 105186

[31] Atif S M, Hussain S and Sagheer M 2019 Effect of viscous dissipation and Joule heating on MHD radiative tangent hyperbolic nanofluid with convective and slip conditions *J. Braz. Soc. Mech. Sci. Eng.* **41** 189

[32] Reddy M G, Vijayakumari P, Krishna L, Kumar K G and Prasannakumara B C 2020 Convective heat transport in a heat generating MHD vertical layer saturated by a non-Newtonian nanofluid: a bidirectional study *Multidiscip. Model. Mater. Struct.* (https://doi.org/10.1108/MMMS-01-2020-0002)

[33] Muhammad N, Nadeem S and Mustafa M T 2018 Analysis of ferrite nanoparticles in the flow of ferromagnetic nanofluid *PLoS One* **13** e0188460

[34] Wang C Y 2002 Flow due to a stretching boundary with partial slip—an exact solution of the Navier–Stokes's equations *Chem. Eng. Sci.* **57** 3745–7